Electronic Supplementary Information For:

Increasing p-type Dye Sensitised Solar Cell Photovoltages using Polyoxometalates

Hani El Moll, Fiona A. Black, Christopher J. Wood, Ahmed Al-Yasari, Anil Reddy Marri, Igor V. Sazanovich, Elizabeth A. Gibson and John Fielden

General

Materials and Procedures. Acetonitrile (MeCN) was freshly distilled under nitrogen from an appropriate drying agent.[1] Dry (sure seal) dimethyl sulfoxide (DMSO) was purchased from Sigma Aldrich, and all preparations of organoimido hexamolybdate derivatives were performed under an atmosphere of dry nitrogen using standard Schlenk techniques. Compound **2** was synthesized by modification of a reported procedure[2] and its identity confirmed by ^{1}H-NMR, as were the precursors tetrabutylammonium hexamolybdate[3] and 4-(4-pyridyl) aniline.[4] All other reagents and solvents were obtained as ACS grade from Sigma Aldrich, Alfa Aesar, Fisher Scientific or Fluorochem and used as supplied.

General Physical Measurements. FT-IR spectra were measured using Perkin Elmer FT-IR spectrum BX and Bruker FT-IR XSA spectrometers. ^{1}H- and ^{13}C-NMR spectra were acquired using Bruker AC 300 (300 MHz) and Bruker Ascend 500 (500 MHz) spectrometers and all shifts are quoted with respect to TMS using the solvent signals as secondary standard (s = singlet, d = doublet, t = triplet, q = quartet, sex = sextet, dt = doublet of triplets, m = multiplet). Some quaternary carbon signals were not observed for the organoimido compounds even after 1064 scans of saturated d_6-DMSO solutions, which gave strong signal for all other ^{13}C resonances. Elemental analyses and accurate mass spectrometry were outsourced to London Metropolitan University, and the UK National Mass Spectrometry Service at Swansea University respectively. UV–Vis spectra were obtained by using an Agilent Cary 60 UV-Vis spectrophotometer. Cyclic voltammetric measurements were carried out using Autolab PGStat 30 potentiostat/galvanostat. A single-compartment or a conventional three-electrode cell was used with a silver/silver chloride reference electrode (3M NaCl, saturated AgCl), glassy carbon or platinum working electrode and Pt wire auxiliary electrode. Acetonitrile was freshly distilled (from CaH_2), $[N(C_4H_9\text{-}n)_4]PF_6$, as supplied from Fluka, and $[N(C_4H_9\text{-}n)_4]BF_4$,[5] were used as the supporting electrolyte. Solutions containing ca. 10^{-3} M analyte (0.1 M electrolyte) were degassed by purging with nitrogen. All $E_{1/2}$ values were calculated from $(E_{pa} + E_{pc})/2$ at a scan rate of 100 mV s^{-1} and referenced to Fc/Fc^{+}. Solar cell assembly, measurements and surface characterization are described below.

Synthetic Methods

Synthesis of $[(C_4H_9)_4N]_2[Mo_6O_{18}NC_6H_4COOH]$ (2).

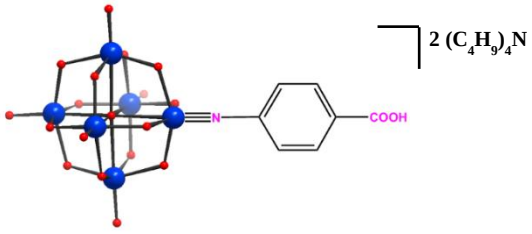

2 was synthesized by modification of a reported procedure. A mixture of 4-aminobenzoic acid (0.274 g, 2 mmol), $(n\text{-}Bu_4N)_2Mo_6O_{19}$ (3.000 g, 2.2 mmol), and DCC (1,3-dicyclohexylcarbodiimide) (0.54 g, 2.6 mmol) was heated in a 30 mL dry DMSO for 5 h at 70 ºC. A rapid colour change to red was observed. After being cooled to room temperature the solution was filtered into a flask containing 400 mL diethyl

ether. An orange precipitate was formed and collected by filtration and then washed generously using diethyl ether. The resulting solid was recrystallized twice from hot acetonitrile and washed with diethyl ether to afford an orange solid (1.6 g, 1.1 mmol, 55 %). The final product was dried under vacuum for 24 hours. ^{1}H NMR (300 MHz, DMSO, 25 ºC): δ= 13.12 (s, 1H, COOH), 7.98 (d, ^{3}J = 8.4 Hz, 2H, arom. CH), 7.28 (d, ^{3}J = 8.4 Hz, 2H, arom. CH), 3.16 (t, ^{3}J = 8.2 Hz, 16H, CH_2) 1.62-1.51 (m, 16H, CH_2), 1.36-1.25 (m, 16H, CH_2), 0.93 (t, ^{3}J = 7.2 Hz, 24H, CH_3).

Synthesis of $[(C_4H_9)_4N]_2[Mo_6O_{18}N_2C_{11}H_8]$ (3).

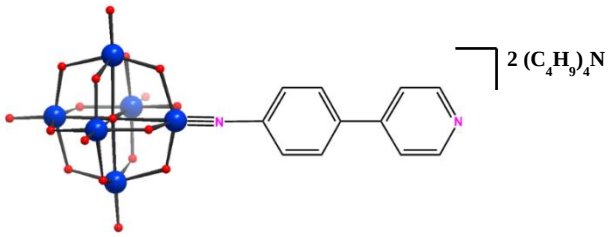

A mixture of 4-pyridyl-4-aniline (0.170 g, 1 mmol), $(n\text{-}Bu_4N)_2Mo_6O_{19}$ (1.770 g, 1.3 mmol), and DCC (1,3-dicyclohexylcarbodiimide) (0.270 g, 1.3 mmol) was heated in a 15 mL dry DMSO for 12 h at 70 ºC. A colour change to red was observed. After being cooled to room temperature the solution was filtered into a flask containing 200 mL diethyl ether. An orange precipitate was formed and collected by filtration and then washed generously using diethyl ether. The resulting solid was recrystallized twice from hot acetonitrile and washed with diethyl ether to afford **3** as an orange solid (0.950 g, 0.63 mmol, 63 %). The final product was dried under vacuum for 24 hours. ^{1}H NMR (300 MHz, DMSO, 25 ºC): 8.64 (d, ^{3}J = 5.4 Hz, 2H, arom. CH), 7.93 (d, ^{3}J = 8.7 Hz, 2H, arom. CH), 7.74 (d, ^{3}J = 5.4 Hz, 2H, arom. CH), 7.34 (d, ^{3}J = 8.4 Hz, 2H, arom. CH), 3.16 (t, ^{3}J = 8.2 Hz, 16H, CH_2) 1.62-1.51 (m, 16H, CH_2), 1.36-1.25 (m, 16H, CH_2), 0.93 (t, ^{3}J = 7.2 Hz, 24H, CH_3). ^{13}C NMR (125 MHz, DMSO, 25 ºC): 150.7, 149.14, 128.23, 127.62, 127.03, 114.54, 58.04, 23.57, 19.69, 13.98. Anal. Calcd (found) % for $C_{43}H_{80}Mo_6N_4O_{18}$: C 34.05 (33.98), H 5.32 (5.38), N 3.69 (3.76). *m/z* = 515.7 $[C_{11}H_8Mo_6N_2O_{18}]^{2-}$.

Synthesis of $[(C_4H_9)_4N]_2[Mo_6O_{18}NC_6H_{10}COOH]$ (4).

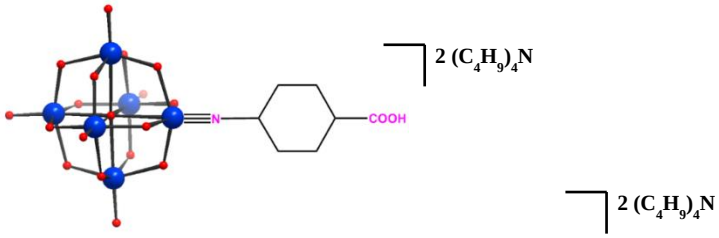

A mixture of cis-4-Aminocyclohexanecarboxylic acid (0.143 g, 1 mmol), $(n\text{-}Bu_4N)_2Mo_6O_{19}$ (1.500 g, 1.1 mmol), and DCC (1,3-dicyclohexylcarbodiimide) (0.27 g, 1.3 mmol) was heated in a 15 mL dry DMSO for 3 h at 65 ºC. A rapid colour change to red was observed. After being cooled to room temperature the solution was filtered into a flask containing 400 mL diethyl ether. An orange precipitate was formed and collected by filtration and then washed generously using diethyl ether. The impurities were recrystallized out from hot acetonitrile and the solvent was reduced under vacuum. If necessary, the product can be purified twice to afford **4** a light orange solid (0.75 g, 0.5 mmol, 50 %). The final product was dried under vacuum for 24 hours. ^{1}H NMR (300 MHz, DMSO, 25 ºC): 3.17 (t, ^{3}J = 8.2 Hz, 16H, CH_2), 2.54 (br., 2H), 1.84-1.70 (m, 3H), 1.62-1.51 (m, 18H), 1.34-1.25 (m, 19H), 0.94 (t, ^{3}J = 7.3 Hz, 24H, CH_3). Anal. Calcd (found) % for $C_{39}H_{83}Mo_6N_3O_{20}$: C 31.44 (31.58), H 5.61 (5.57), N 2.82 (2.88). *m/z* = 502.2 $[C_7H_{11}Mo_6NO_{20}]^{2-}$.

X-ray Crystallography

Sample Growth, Data Collection and Refinement. X-ray diffraction quality crystals of **3** were obtained by room temperature diffusion of diethyl ether vapour into acetonitrile. Data reduction, cell refinement and absorption correction was carried out using Agilent Technologies CrysAlisPro[6] and the structure was solved using SIR-92[7] *via* WinGX.[8] Refinement was achieved by full-matrix least-squares on all F_0^2 data using SHELXL-2014.[9] Full crystallographic data and refinement details are presented in Table S1. The asymmetric unit contains the complete molecular anion and both cations, see Figure S1.

Table S1. Crystallographic Data and Refinement Details for $[(C_4H_9)_4N]_2[Mo_6O_{18}N_2C_{11}H_8]$ (**3**)

Formula	$C_{43}H_{80}Mo_6N_4O_{18}$
M	1516.75
Crystal system	Mono clinic
Space group	$P2_1/n$
a/Å	11.6722(4)
b/Å	34.0516(16)
c/Å	14.1145(6)
α/deg	90
β/deg	91.962(3)
γ/deg	90
V/Å^3	5606.6(4)
Z	4
T/K	140(2)
μ/mm^{-1}	1.370
Cryst. size/mm	0.190 x 0.120 x 0.030
Cryst. description	Orange
No. reflns collected	55034
No. of indep. reflns (R_{int})	12870 [R(int) = 0.0597]
θ_{max}/deg (completeness)	99.8%
Reflections with $I > 2\backslash(I)$	8937
Goodness-of-fit on F^2	1.016
Flack parameter	N/A
final R_1, wR_2 [I > 2sigma(I)]	R1 = 0.0428, wR2 = 0.0715
(all data)	R1 = 0.0799, wR2 = 0.0789
Peak and hole/e Å^{-3}	0.862 and -0.671

Structure and selected Bond Lengths and Angles. ORTEP representation of the asymmetric unit of compound **3** is shown below in Figure S2. Selected bond lengths and angles in the anions are listed in Table S2. The Mo-N-C bond angle is closer to 180˚ than 120˚, indicating significant Mo-N triple bond character. The compounds also show the typical imido-Lindqvist pattern of a shortened bond length from the imido-Mo (Mo^{im}) to the central oxygen (O^c), lengthened equatorial bond lengths from Mo^{im} to the oxygens bridging (O^b), lengthened bond lengths from the belt Mo positions (Mo^b) to the O^b, lengthened bond lengths from the Mo^b to the terminal oxygens (O^t), a lengthened axial bond length from the *trans*-Mo (Mo^t) to O^c and a lengthened axial bond length from Mo^t to O^t.[10]

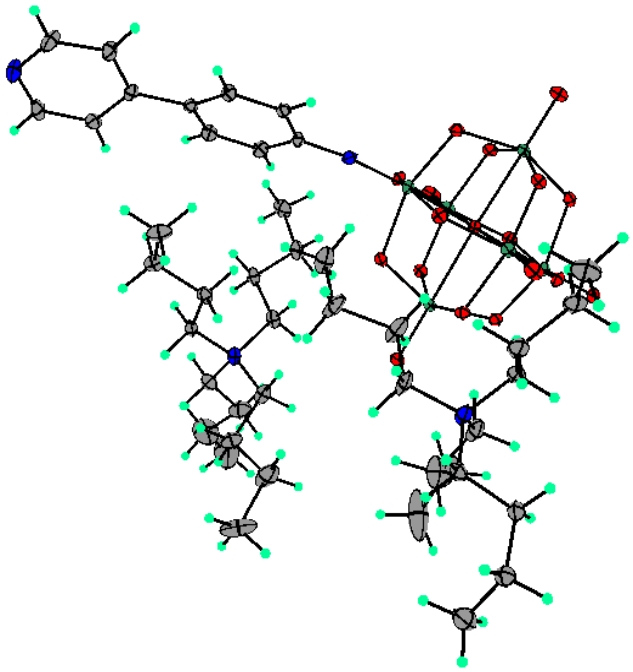

Figure S1. ORTEP representation of the asymmetric unit in **3**. Thermal ellipsoids are at the 30% probability level. Colour scheme: Mo, green; O, red; C, gray; N, blue; H atoms are represented by light green circles of arbitrary radii.

Table S2. Selected bond lengths (Å) and angles (°) in the anion of compound **3**. Mo^{im} – imido bearing Mo; Mo^{b},belt Mo; Mo^{t}, *trans*-Mo; O^{c}, central O; O^{b}, bridging O; O^{t}, terminal O.

Atoms	**Distance (Å) or Angle (°)**
C-N-Mo^{im}	170.6(4)
N-Mo^{im}	1.740(3)
Mo^{im}-O^{c}	2.197(3)
Mo^{im}-O^{b} (average)	1.955(1)
Mo^{b}-O^{c} (average)	2.337(1)
Mo^{b}-O^{b} (average)	1.941(6)
Mo^{b}-O^{t} (average)	1.688(6)
Mo^{t}-O^{c}	2.371(3)
Mo^{t}-O^{b} (average)	1.921(1)
Mo^{t}-O^{t}	1.689(3)

Electronic Spectra and Electrochemistry of 1 to 4

As commonly seen in arylimido Lindqvist compounds,[10] **2** and **3** both show strong charge transfer bands (ligand to polyoxometalate charge transfer, LPCT) in the near-UV to visible part of the spectrum (Figure S2, Table S3). However, alkyl imido derivative **4** shows a UV-vis absorption profile that is only minimally changed from that of $[NBu_4]_2[Mo_6O_{19}]$ (**1**). The imido-derivatives **2** to **4** also show the typical negative shift in reduction potentials, associated with higher electron density being pushed onto the $\{Mo_6\}$ cluster when the organic moiety is attached. This shift is larger (*ca.* 300 mV) for the cyclohexyl derivative **4**, than for the arylimido derivatives **2** and **3** because of the higher electron donating ability of the cyclohexyl group. Logically, the smallest shift occurs for **3** which contains an electron deficient pyridyl ring. Compound **3** also shows an irreversible reduction associated with the pyridyl group.

Table S3 UV-vis Absorption and Electrochemical Data for **1** to **4** in acetonitrile

Compound	λ_{max}, nm[a] (ε , 10^3 M^{-1} cm^{-1})	Assignment	$E_{1/2}$, V vs Ag/AgCl (ΔE_p, mV)[b] or E_{pc}, V
1	223 (24.9) 261 (13.4) 323 (7.1)	O→Mo O→Mo O→Mo	-0.315 (69)
2	218 (20.0) 229 (21.8) 258 (25.5) 352 (18.2)	O→Mo/π→π* O→Mo/π→π* O→Mo/π→π* LPCT	-0.507 (106)
3	218 (41.7) 279 (38.4) 362 (30.6)	O→Mo/π→π* O→Mo/π→π* LPCT	-0.483 (78) -1.348[c]
4	220 (28.8) 255 (16.7) 325 (8.3)	O→Mo O→Mo O→Mo/N→Mo	-0.607 (94)

[a] Concentrations *ca.* 10^{-5} M in MeCN. [b] Solutions *ca.* 10^{-3} M in analyte and 0.1 M in $[NBu_4][BF_4]$ at a glassy carbon working electrode with a scan rate of 100 mV s^{-1}. Ferrocene internal reference $E_{1/2}$ = 0.46 V, ΔE_p = 80 mV. [c]Irreversible reduction of pyridyl group.

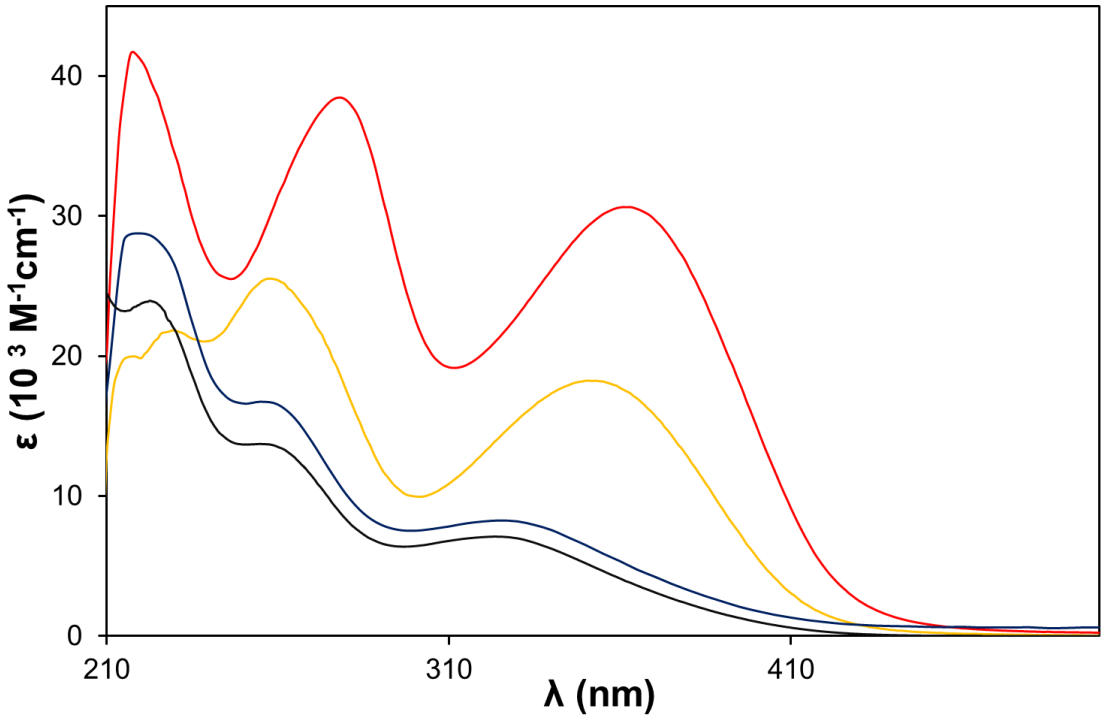

Figure S2 UV-visible absorption spectra of POM compounds in acetonitrile at 298 K: **1** ($[NBu_4]_2[Mo_6O_{19}]$, black); **2** ($[(NBu_4)_2[Mo_6O_{18}NPhCO_2H]$, yellow); **3** ($[(NBu_4)_2[Mo_6O_{18}NPhPy]$, red) and **4** ($[(NBu_4)_2[Mo_6O_{18}NCyCO_2H]$, blue).

NiO film, Solar Cell, and Transient Absorption Studies

Solar Cell Assembly and Measurements. A NiO precursor solution was prepared by dissolving anhydrous $NiCl_2$ (1 g) and the tri-block co-polymer F108 (poly(ethylene glycol)-block-poly (propylene glycol)-block-poly(ethylene glycol)) (1 g) in ethanol (6 g) and distilled water (5 g). The solution was allowed to rest for 10 days and then centrifuged to separate out any remaining solids.

For the photocathodes, conducting glass substrates (Pilkington TEC15, sheet resistance 15 Ω/square) were cut to size (approx. 2 × 2 cm) and then cleaned by sonic bath for 15 minutes, first in soapy water, second in 0.1 M HCl, and finally in ethanol. The NiO electrodes were made by applying the precursor solution onto the conducting glass substrates by doctor blade using Scotch Magic tape as a spacer (0.2 cm^2 active area), followed by sintering in a Nabertherm B150 oven at 450 °C for 30 min. Additional layers of precursor solution were applied and sintered to increase the film thickness. The NiO electrodes were soaked in a dichloromethane (or acetonitrile) solution of the dye (0.3 mM) for 16 h at room temperature. Where used, POM coadsorbents were applied by soaking the dyed NiO electrodes in acetonitrile solutions of **1** to **4** (0.3 mM). For the counter electrodes, the conducting glass substrates (Pilkington TEC8, sheet resistance 8 Ω/square) were cut and cleaned as described above. A small (*ca.* 1 × 1 mm) hole was drilled into a corner for the electrolyte solution to be introduced at the assembly stage. Platinized counter electrodes were prepared by applying chloroplatinic acid solution (4.4 mM, 10 μL cm^{-2}) in ethanol onto the conducting glass substrate. The electrodes were then heated in a Nabertherm B150 oven at 400 °C for 15 minutes and then allowed to cool. The dyed electrodes were removed from the dye bath and washed with acetonitrile. Cells were assembled face-to-face with the platinized counter electrode using a 30 μm thick thermoplastic frame (Surlyn 1702). The electrolyte contained LiI (1.0 M) and I_2 (0.1 M) in dry acetonitrile (or propylene carbonate), or $Co^{II}(tBBPy)_3(ClO_4)_2$ (0.1M), $Co^{III}(tBBPy)_3(ClO_4)_3$ and LiClO4 (0.1M) in propylene carbonate, and was introduced through the predrilled hole in the counter electrode by vacuum back filling. The cells were then sealed using a 30 μm thick thermoplastic square (Surlyn 1702) and a glass cover slip.

Current density vs. voltage measurements were measured using an Ivium CompactStat potentiostat either in the dark or under AM 1.5 simulated sunlight from an Oriel 150 W solar simulator, calibrated using a Si diode to give light with an intensity of 100 mW cm^{-2}. DSCs were held in place using a custom made cell holder with a circular aperture with a diameter 1 mm wider than the working area of the cell. An applied voltage was swept from slightly above the given open-circuit voltage, at a scan rate of 3 mV s^{-1}. Incident photon-to- current conversion efficiencies (IPCEs) were recorded by passing the light from the solar simulator through an Oriel Cornerstone 130 1/8 m monochromator over the range of 400-700 nm at 10 nm increments and recording the current from the solar cell with an Ivium CompactStat potentiostat which was calibrated against a Si photodiode. Small amplitude square wave modulated (SSWM) photovoltage and photocurrent experiments were performed on the same p-DSC devices used for photocurrent−photovoltage (JV) and IPCE measurements at open circuit and short circuit, respectively. SSWM experiments were done over a range of light intensities, using an Ivium Modulight as a modulated light source with a 10% modulation of light intensity. The photovoltage and photocurrent rise and decays were recorded using an Ivium CompactStat potentiostat; the lifetimes were fitted to a first-order exponential decay using Origin Pro 8. Charge extraction was performed using the same equipment. The cell was illuminated at open-circuit until a constant V_{OC} was reached. The light source was then switched off, allowing for a decay in photovoltage over a range of time intervals. Then the cell was switched to short-circuit conditions and the current response was recorded. The current decay over 10 s was integrated to give the charge at varying bias.

Surface Elemental Analysis of POM treated NiO films. EDX analysis was conducted on a subset of films (NiO, NiO|P1, NiO|**3**, NiO|P1|**1**, NiO|P1|**2**, NiO|P1|**3** and NiO|P1|**4**) using an FEI NanoSEM SEM/EDX. While EDX is not necessarily reliable as a means to quantify the absolute level of molybdenum in the films (due to dependence on the type of substrate), presence of Mo in the POM

modified films and absence from the others confirms that POM is adsorbed. The similarity between the samples, in terms of level of Mo, and Ni:Mo ratios (Table S4 and S5), implies that binding of the POMs is controlled more by charge and size (POMs are negatively charged and NiO carries a positive surface charge) than by specific interactions between NiO and organic binding groups.

Table S4 EDX surface analysis results in atomic % for a selection of POM treated, and POM free NiO films. For each individual film, values are the average (mean) of 5 or more points on the film, overall values are the mean of the three individual films.

	C	**O**	**Si**	**Ni**	**Mo**	**Sn**
NiO mean	**4.51**	**72.1**	**1.52**	**15.47**	**0**	**5.67**
NiO|P1 mean	**7.05**	**71.53**	**1.60**	**13.26**	**0**	**5.89**
NiO|P1|**1** Film 1 mean	10.75	62.67	0.58	22.56	0.50	3.26
NiO|P1|**1** Film 2 mean	5.75	71.82	1.60	14.19	0.22	6.3
NiO|P1|**1** Film 3 mean	7.91	66.24	0.71	19.90	0.33	4.76
NiO|P1|1 overall mean	**8.14**	**66.91**	**0.96**	**18.88**	**0.35**	**4.77**
NiO|P1|**2** Film 1 mean	9.41	66.06	0.79	19.13	0.31	4.44
NiO|P1|**2** Film 2 mean	10.29	63.83	0.6	20.16	0.34	4.35
NiO|P1|**2** Film 3 mean	8.64	67.50	1.21	16.73	0.33	5.41
NiO|P1|2 overall mean	**9.45**	**65.80**	**0.87**	**18.67**	**0.33**	**4.73**
NiO|P1|**3** Film 1 mean	3.96	73.60	1.7	14.05	0.23	6.46
NiO|P1|**3** Film 2 mean	5.48	71.91	1.58	14.76	0.25	6.02
NiO|P1|**3** Film 3 mean	5.44	72.00	1.71	14.55	0.23	6.05
NiO|P1|3 overall mean	**4.96**	**72.50**	**1.66**	**14.45**	**0.24**	**6.18**
NiO|P1|**4** Film 1 mean	8.73	67.23	1.07	17.88	0.31	4.78
NiO|P1|**4** Film 2 mean	6.87	68.38	1.06	18.15	0.26	5.18
NiO|P1|**4** Film 2 mean	10.77	64.99	1.19	16.61	0.59	5.27
NiO|P1|4 overall mean	**8.79**	**66.87**	**1.11**	**17.55**	**0.38**	**5.08**
NiO|**3**	5.35	69.86	0.78	19.86	0.39	4.77
NiO|**3**	4.33	71.50	1.25	17.15	0.30	5.47
NiO|**3**	4.90	69.78	0.85	19.13	0.34	5.00
NiO|3 overall mean	**4.86**	**70.38**	**0.96**	**18.71**	**0.34**	**5.08**

Table S5 Average Ni:Mo ratios for each type of film showing relatively small variation between the POM treated systems.

	Ni:Mo
NiO	-
NiO|P1	-
NiO|P1|**1**	53.9
NiO|P1|**2**	56.6
NiO|P1|**3**	60.2
NiO|P1|**4**	46.2
NiO|**3**	55.0

I-V Curves. Below current-voltage curves are displayed for the cells tabulated in the main paper

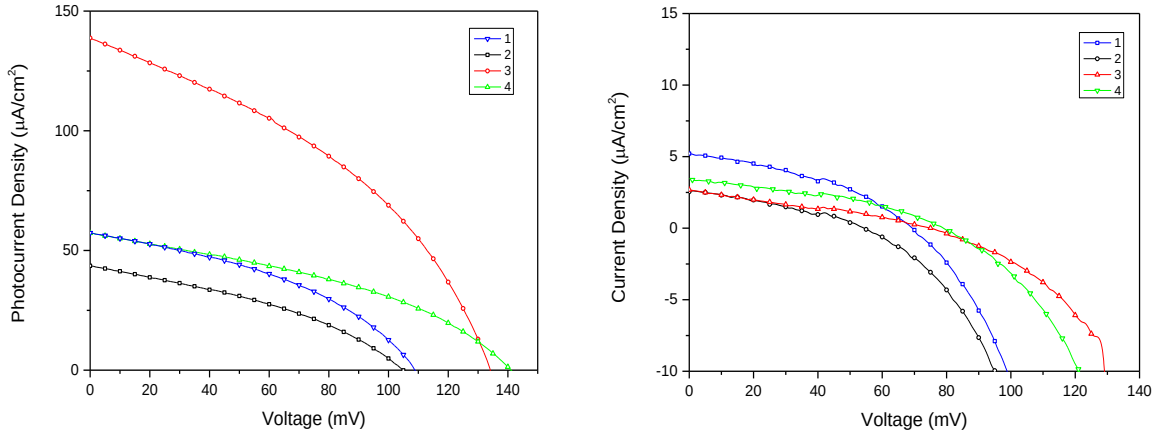

Figure S3 Current-voltage plots measured for NiO|POM cells with I^-/I_3^- electrolyte. Left: under AM1.5 irradiation (100 mW cm^{-2}); Right: in the dark.

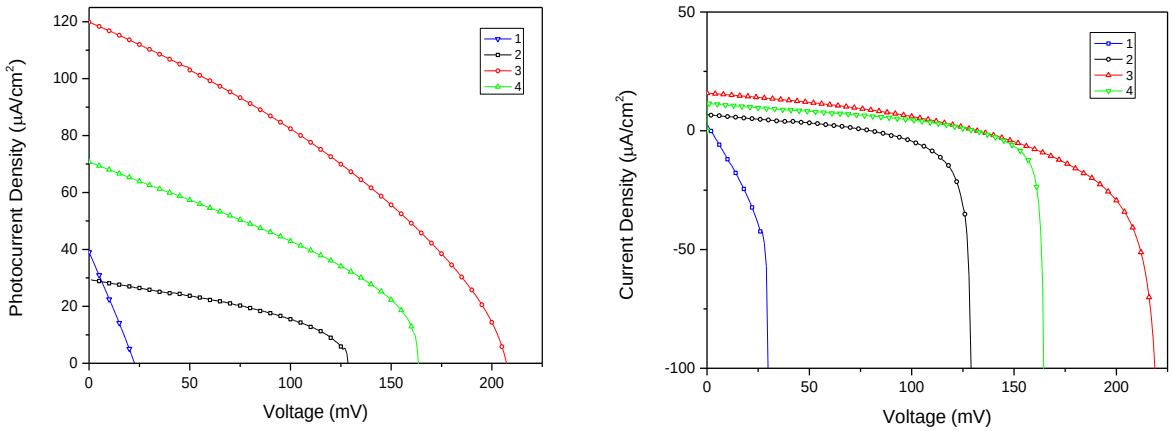

Figure S4. Current-voltage plots measured for NiO|POM cells with $Co(tBBPY)_3^{2+/3+}$ electrolyte. Left: under AM1.5 irradiation (100 mW cm^{-2}); Right: in the dark.

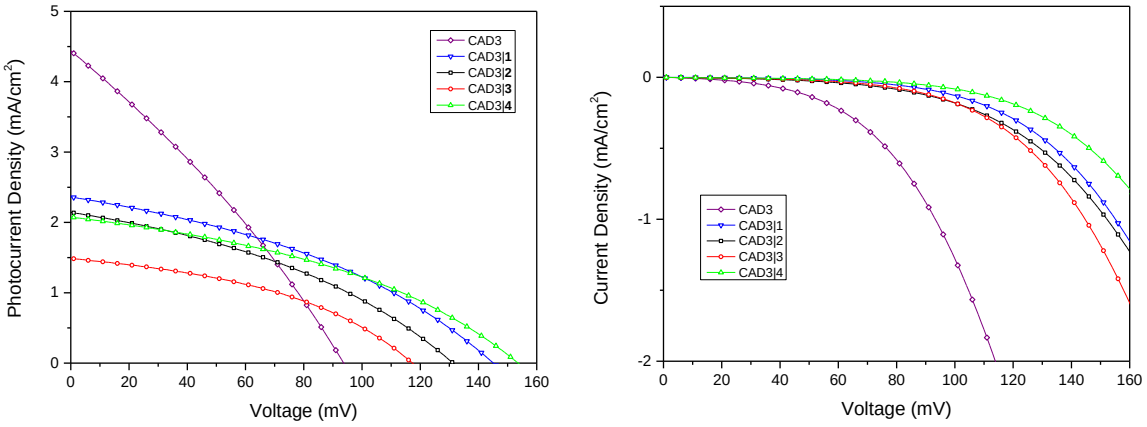

Figure S5. Current density-voltage plots measured for NiO|CAD3|POM cells with I^-/I_3^- electrolyte, where POM_S were coadsorbed with the sensitiser. Left: under AM1.5 irradiation (100 mW cm^{-2}); Right: in the dark.

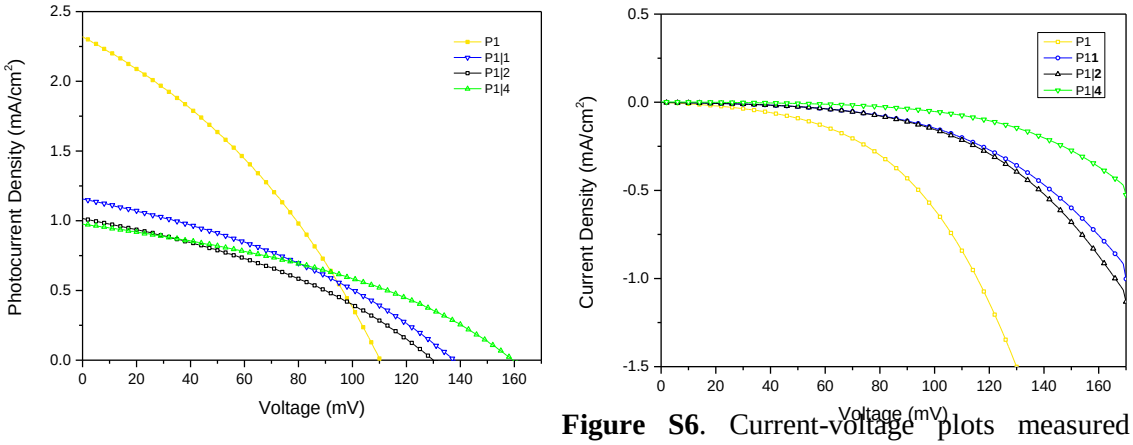

Figure S6. Current-voltage plots measured for NiO|P1|POM cells with I^-/I_3^- electrolyte, where POMs were co-adsorbed with the sensitiser. Left: under AM1.5 irradiation (100 mW cm^{-2}); Right: in the dark.

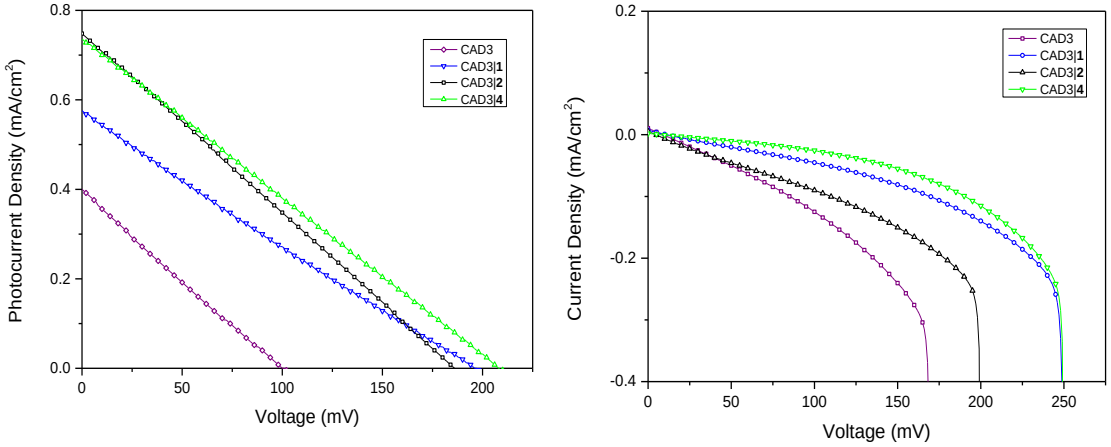

Figure S7. Current-voltage plots measured for NiO|CAD3|POM cells with $Co(tBBPY)_3^{2+/3+}$ electrolyte, where POMs were co-adsorbed with the sensitiser. Left: under AM1.5 irradiation (100 mW cm^{-2}); Right: in the dark.

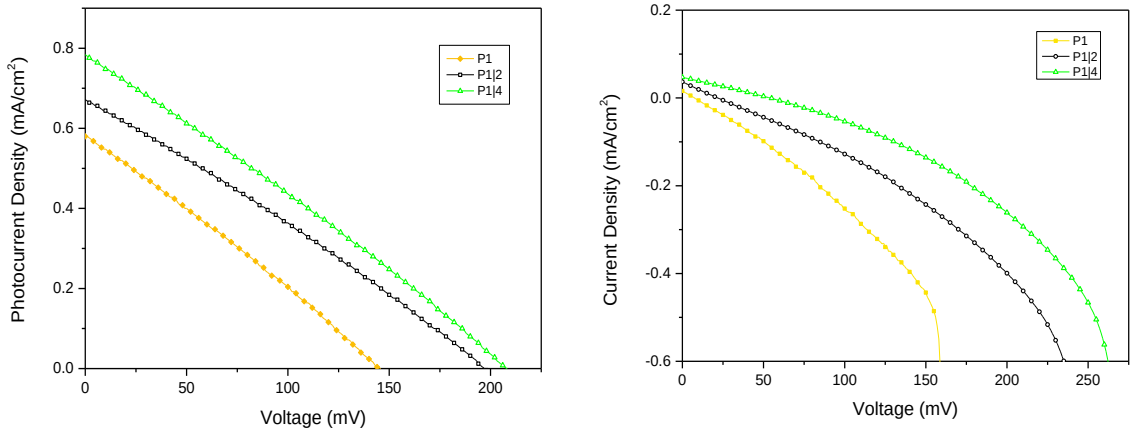

Figure S8. Current-voltage plots measured for NiO|P1|POM cells with $Co(tBBPY)_3^{2+/3+}$ electrolyte, where POMs were co-adsorbed with the sensitiser. Left: under AM1.5 irradiation (100 mW cm^{-2}); Right: in the dark.

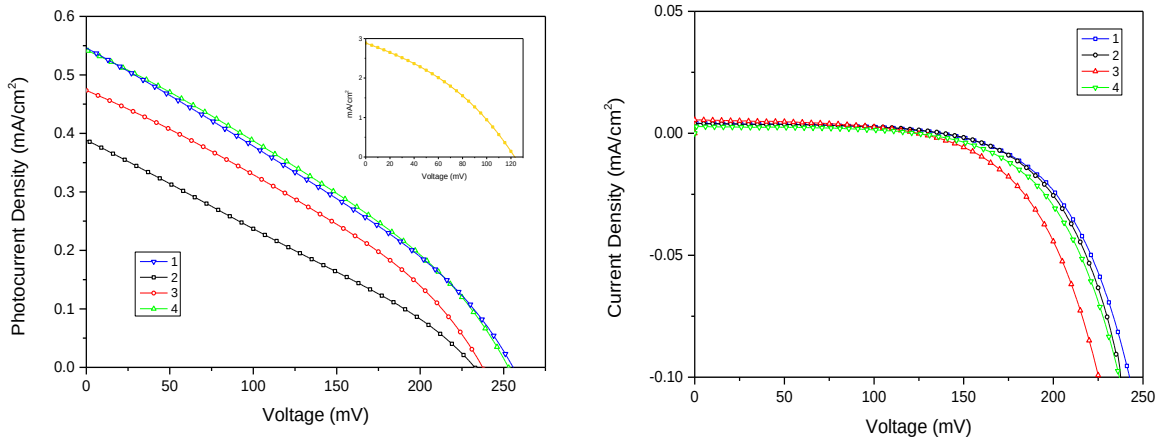

Figure S9. Current-voltage plots measured for NiO|P1 cells with a POM/I^-/I_3^- electrolyte and an I^-/I_3^- electrolyte (inset). Left: under AM1.5 irradiation (100 mW cm^{-2}); Right: in the dark.

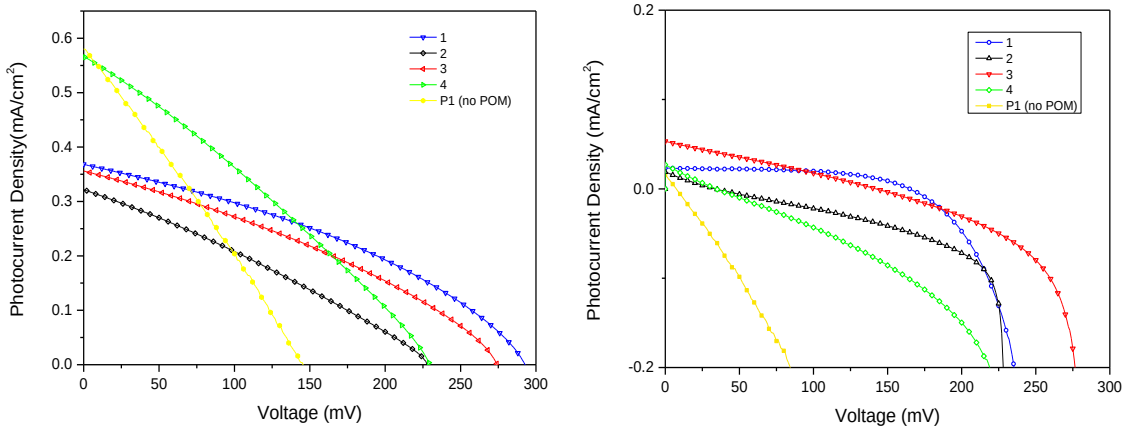

Figure S10. Current-voltage plots measured for NiO|P1 cells with a POM/$Co^{2+/3+}$ electrolyte. Left: under AM1.5 irradiation (100 mW cm^{-2}); Right: in the dark.

Extracted Charge vs Charge Density

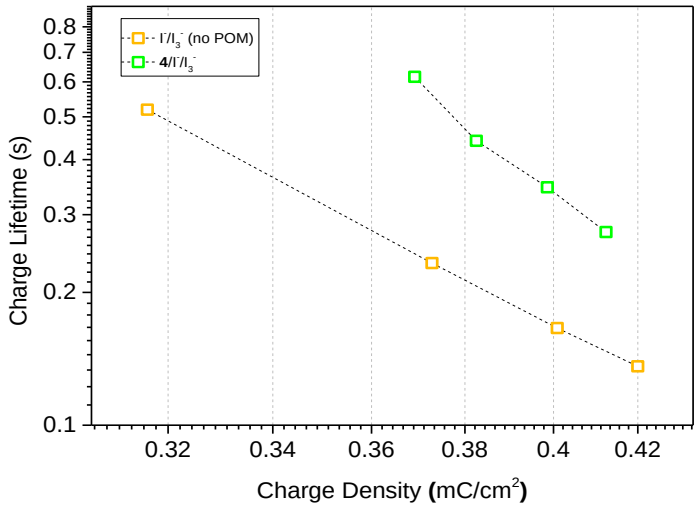

Figure S11. Charge lifetime vs extracted charge of NiO|P1 cells, with and without **4** added to I^-/I_3^- electrolyte. We note that the valence band shift of the oxide will have influenced charge lifetimes,

however, a large difference in charge between POM containing and POM free-systems has prevented satisfactory estimation of the shift. Therefore, this data should be interpreted qualitatively.

Time-Resolved Infra-Red Spectroscopy. The nanoporous NiO films were prepared by spraying a saturated solution of $NiCl_2$ in acetylacetone onto the surface of the CaF_2 window (Crystran), which was preheated to 450 °C on a hot plate. This was then allowed to cool slowly to room temperature to give a compact film of NiO. The mesoporous layer was then deposited on top of the compact layer using the F108-templated precursor solution described above. The film was sintered at 450 °C for 30 min, and an additional layer of precursor solution was applied and sintered to increase the film thickness. The windows were then immersed in a solution of P1 for 12 hours. For measurements involving polyoxometalate, the dyed P1|NiO films were additionally dyed in a solution of **4** for 12 hours. Spectra were recorded in solution cells (Harrick Scientific Products Inc.) with CaF_2 windows and a 490 μm Teflon spacer.

Picosecond Time-Resolved Infra-Red (TRIR) spectra were recorded using the ULTRA instrument located in the Central Laser Facility at the Rutherford Appleton Laboratory. Briefly, two titanium sapphire dual output amplifiers (Thales) of 10 kHz and 1 kHz were synchronized using a common 65 MHz oscillator. The 1 kHz output was used as a pump and the 10 kHz as probe.data recording scheme. The pump laser was tuned to 532 nm by optical parametric amplification (OPA, Light Conversion, TOPAS) and the mid-IR probe pulses were generated using OPA with difference frequency mixing. For all measurements the pump polarization was set to magic angle relative to the probe. The IR probe beam was split to form reference and probe beams which were passed through spectrographs onto MCT array detectors (IR Associates). High speed data acquisition systems (Quantum Detectors) allowed 10 kHz acquisition and processing of the probe and reference pulses to generate a pump-on pump-off infrared absorption difference signal. The spot sizes in the sample region were ca. 150 and 50 μm for the pump and probe, respectively, with pump energies of 50 nJ. The cell was rastered in the two dimensions orthogonal to the direction of beam propagation to minimize localized sample decomposition.

References

1. W. L. F. Armarego and C. L. L. Chai, *Purification of laboratory chemicals*; 6th ed.; Elsevier/Butterworth-Heinemann: Amsterdam; Boston, 2009.

2. Y. Zhu, P. Yin, F. Xiao, D. Li, E. Bitterlich, Z. Xiao, J. Zhang, J. Hao, T. Liu, Y. Wang, and Y. Wei, *J. Am. Chem. Soc.*, 2013, **135**, 17155.

3. W. G. Klemperer, *Inorg. Synth.* 1990, **27**, 71.

4. V. L. Gunderson, A. L. Smeigh, C. H. Kim, D. T. Co, and M. R. Wasielewski, *J. Am. Chem. Soc.*, 2012, **134**, 4363.

5. S. K. Ibrahim, Ph.D Thesis, University of Sussex, 1992.

6. *CrysAlisPro* (Version 1.171.36.21), Agilent Technologies, Inc.; Santa Clara: CA, United States, 2012.

7. A. Altomare, G. Cascarano, C. Giacovazzo, A. Guagliardi, M. C. Burla, G. Polidori, M. Camalli, *J. Appl. Cryst.* 1994, **27**, 435.

8. L. J. Farrugia, *J. Appl. Cryst.* 1999, **32**, 837.

9. G. M. Sheldrick, *SHELXL-2014*, Programs for Crystal Structure Analysis (Release 2014-7); University of Göttingen: Göttingen, Germany, 2014.

10. (a) A. Al-Yasari, N. Van Steerteghem, H. El Moll, K. Clays and J. Fielden, *Dalton Trans.*, 2016, **45**, 2818. (b) Y. Wei, B. Xu, C. L. Barnes and Z. Peng, *J. Am. Chem. Soc.* 2001, **123**, 4083. (c) B. Xu, Y. Wei, C. L. Barnes and Z. Peng, *Angew. Chem. Int. Ed.* 2001, **40**, 2290. (d) J. B. Strong, G. P. A. Yap, R. Ostrander, L. M. Liable-Sands, A. L. Rheingold, R. Thouvenot, P. Gouzerh and E. A. Maatta, *J. Am. Chem. Soc.* 2000, **122**, 639.